ChemPubSoc Europe

DOI: 10.1002/cmdc.201700228

CHEMMEDCHEM Full Papers

Development of a New Structural Class of Broadly Acting HCV Non-Nucleoside Inhibitors Leading to the Discovery of MK-8876

Casey C. McComas,*[a] Anandan Palani,[a] Wei Chang,[b] M. Katharine Holloway,[a] Charles A. Lesburg,[a] Peng Li,[b] Nigel Liverton,[a] Peter T. Meinke,[a] David B. Olsen,[a] Xuanjia Peng,[b] Richard M. Soll,[b] Ajay Ummat,[a] Jie Wu,[b] Jin Wu,[a] Nicolas Zorn,[a] and Steven W. Ludmerer[a]

Studies directed at developing a broadly acting non-nucleoside inhibitor of HCV NS5B led to the discovery of a novel structural class of 5-aryl benzofurans that simultaneously interact with both the palm I and palm II binding regions. An initial candidate was potent in vitro against HCV GT1a and GT1b replicons, and induced multi-log reductions in HCV viral load when orally dosed to chronic GT1 infected chimpanzees. However, in vitro potency losses against clinically relevant GT1a variants prompted a further effort to develop compounds with sustained potency across a broader array of HCV genotypes and mutants. Ultimately, a biology and medicinal chemistry collaboration led to the discovery of the development candidate MK-8876. MK-8876 demonstrated a pan-genotypic potency profile and maintained potency against clinically relevant mutants. It demonstrated moderate bioavailability in rats and dogs, but showed low plasma clearance characteristics consistent with once-daily dosing. Herein we describe the efforts which led to the discovery of MK-8876, which advanced into Phase 1 monotherapy studies for evaluation and characterization as a component of an all-oral direct-acting drug regimen for the treatment of chronic HCV infection.

Introduction

The global prevalence of hepatitis C (HCV) infection is estimated to be nearly 3% of the world's population.[1] The morbidity associated with chronic HCV infection includes cirrhosis, fibrosis, and liver failure. In addition, chronic HCV infection is a leading cause of liver transplantation.[2] Recently, a number of therapeutic regimens consisting entirely of orally bioavailable, direct-acting antiviral agents have demonstrated high response rates and have been approved for treatment.[3–5]

The hepatitis C virus is a positive-strand RNA virus which has a high degree of genetic heterogeneity as manifested in the classification of seven major genotypes and multiple subtypes, with considerable additional genetic variability within each class.[6,7] The gene product of the virally encoded NS5B is an RNA-dependent RNA polymerase. Polymerase activity can be enzymatically disrupted by nucleoside analogues through incorporation into the nascent RNA genome, resulting in premature chain termination.[8] In addition to nucleoside analogue inhibitors, multiple classes of non-nucleoside inhibitors (NNIs) have been identified which interact with one of multiple binding sites mapped to various pockets near the enzyme surface.[9] It has been proposed that some of these inhibitors modulate allosteric interactions of the enzyme, resulting in losses of replication capacity.[10] Several of these inhibitors have been clinically validated.[9] These NNI binding pockets typically are less genetically constrained than the active site pocket. A consequence is that breadth of potency across genotypes has been difficult to achieve with these types of inhibitors, many displaying a fragile profile with respect to the emergence of viral resistance. To date only dasabuvir[3] (in combination the protease inhibitor paritaprevir (boosted with ritonavir), the NS5A inhibitor ombitasvir, and ribivarin), and beclabuvir[11] (in combination with the protease inhibitor asunaprevir and the NS5A inhibitor daclatasvir) are non-nucleoside inhibitors approved as a component of a multi-drug regimen, both indicated for the treatment of GT1-infected patients only.

The topology of the NS5B protein is generally likened in shape to that of a right hand with the active site located in the region at the top of the palm. There are four well studied allosteric binding sites conventionally referred to as the thumb I, thumb II, palm I, and palm II sites.[9] The palm II binding site possesses high sequence conservation across genotypes, making it an attractive target for development of a drug that is effective against all HCV genotypes. The initial clinical valida-

[a] Dr. C. C. McComas, Dr. A. Palani, Dr. M. K. Holloway, Dr. C. A. Lesburg, Dr. N. Liverton, Dr. P. T. Meinke, Dr. D. B. Olsen, Dr. A. Ummat, Dr. J. Wu, Dr. N. Zorn, Dr. S. W. Ludmerer
Merck & Co. Inc., Kenilworth NJ (USA)
and
Present address: International Discovery Service Unit, WuXi AppTec, Inc., 1690 Sumneytown Pike, Suite 150, Lansdale, PA 19446 (USA)
E-mail: casey.mccomas@wuxiapptec.com

[b] Dr. W. Chang, Dr. P. Li, Dr. X. Peng, Dr. R. M. Soll, Dr. J. Wu
WuXi AppTec, Shanghai (China)

The ORCID identification number(s) for the author(s) of this article can be found under https://doi.org/10.1002/cmdc.201700228.

tion for NS5B as a drug target for non-nucleoside inhibitors was achieved with HCV-796, a palm II binder, which progressed to Phase 2 studies before being halted due to safety liabilities.[12] Based on these potency data we set out to develop compounds that would inhibit HCV NS5B by binding the palm II site while retaining potent activity against all of the clinically relevant major genotypes. Similar strategies conducted in parallel to this work have recently been described.[13,14]

Results and Discussion

While numerous researchers have investigated derivatives of HCV-796 as potential inhibitors of NS5B, we recognized that the 5-position of the benzofuran core represented an area that had remained largely unexplored.[15] Despite the introduction of alkyl and alkoxy derivatives at this position, no examples of analogues bearing aryl groups at this site were reported. To determine if 5-aryl derivatives would impart a viable path toward developing superior inhibitors, the parent phenyl analogue was synthesized (Scheme 1). 5-Phenyl analogue **1** showed very promising activity with an EC_{50} of 185 nM against the HCV GT1b replicon. This result led us to undertake a program to fully explore the new 5-aryl benzofurans as a chemical scaffold.

Commencing from **1** as a lead, we first probed the effects of varying the pendant alkyl group attached to the sulfonamide. Previous work in our group had established that the ethanolic group posed a significant development liability because one of the primary metabolites of HCV-796 was its oxidation to the aldehyde. More specifically, the prevalence of this reactive aldehyde metabolite posed a potential toxicity risk so an alternative group with a superior profile was attractive. An array of alternative R-groups was examined (Table 1) and it was evident from early SAR studies that diverse motifs were tolerated at this position. While a number of analogues with extended side chains, aryl groups, or heterocycles showed good potency such as **1d** and **1c**, these analogues generally suffered from poor metabolic stability. However, a simple methyl analogue (**1a**) displayed promising potency and attractive overall stability, and was selected as the standard for further optimization.

Holding the *N*-methyl methanesulfonamide constant, the 5-aryl position of the benzofuran was extensively explored. However, to fully optimize the 5-position, it was necessary to develop a versatile synthesis of a fully functionalized intermediate that would allow ready access to a diverse array of aryl analogues. The optimized synthesis is shown in Scheme 2.[16] Starting with 2-hydroxyphenyl acetic acid, selective bromination at the 4-position provided intermediate **3** which was then treated with TBSCl to give silyl ether **4**. Acylation with 4-fluorophenyl acetyl chloride gave intermediate **5** followed by deprotection of the phenol and cyclization under acidic conditions which generated the benzofuran **7**. Nitration of the benzofuran generated intermediate **8**. This was followed by reduction to provide aniline **9**, which was then converted into the methyl sulfonamide **10**. Subsequent hydrolysis of the ester and condensation with methyl amine provided amide **12** with all key functionalities in place. Alkylation of **12** allowed ready access to key intermediate benzofuran core **13**. The key core **13** was an excellent substrate for Suzuki coupling and was used for the facile exploration of a range of 5-aryl substituents. Alternatively, **13** could be readily converted into

Table 1. Anti-HCV replicon activity of sulfonamide derivatives of compound **1**.

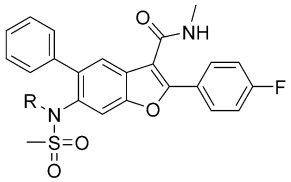

Compd	R	EC_{50} [nM][a] GT1b	GT2a
HCV-796		8	31
1	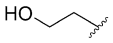	62	185
1a		120	ND
1b		29	98
1c	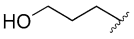	12	62
1d	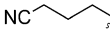	9	37
1e	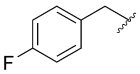	125	338
1f	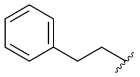	145	602
1g	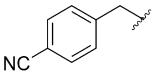	50	>250
1h	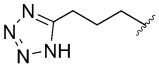	>1000	>1000
1i	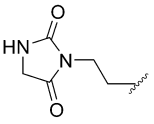	118	250

[a] Data are the mean of $n \geq 2$ determinations unless otherwise noted; ND = not determined.

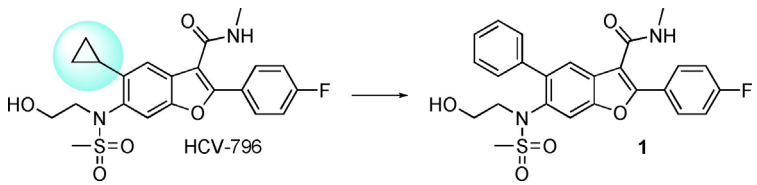

Scheme 1. Novel 5-aryl-substituted benzofurans.

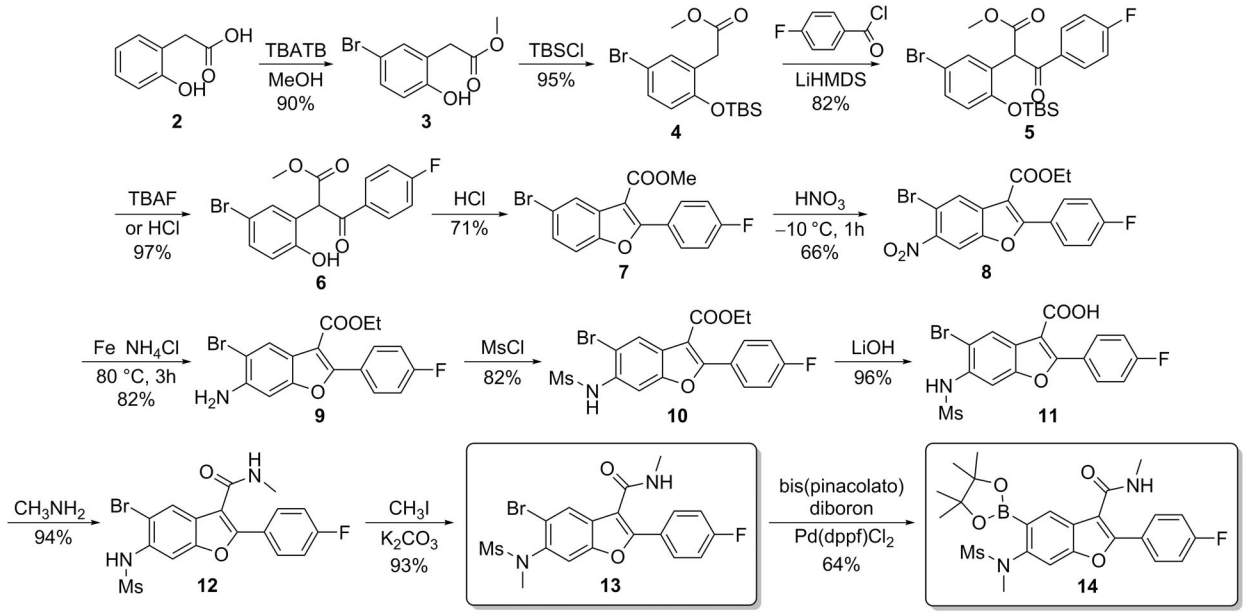

Scheme 2. Synthesis of key intermediates **13** and **14**.

Table 2. Anti-HCV replicon activity of 5-aryl-substituted analogues of **1a**.

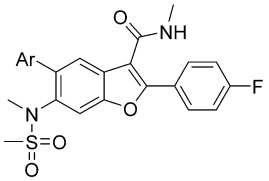

Compd	Ar	EC_{50} [nM][a] GT1b	GT2a	Compd	Ar	EC_{50} [nM][a] GT1b	GT2a
1a		120	ND	**14h**	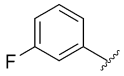	22	129
14a	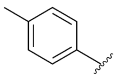	25	69	**14i**		156	139
14b	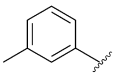	32	923	**14j**	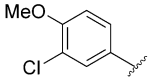	6	96
14c		109	1790	**14k**	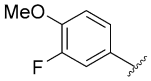	6	72
14d	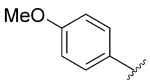	16	60	**14l**[b]	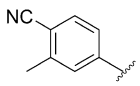	25	111
14e	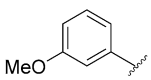	24	48	**14m**[b]	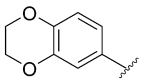	17	127
14f	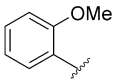	133	348	**14n**[b]	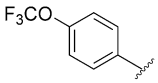	83	169
14g	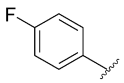	22	48	**14o**[b]	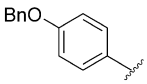	76	270

[a] Data are the mean of $n \geq 2$ determinations unless otherwise noted; ND = not determined. [b] $n = 1$.

boronate **14** to generate more complex 5-aryl derivatives.

With the key bromobenzofuran intermediate **13** now readily available, a range of 5-aryl derivatives was generated to further explore the SAR at this position (Table 2). A number of these analogues showed promising activity and identified clear SAR trends. In general, *ortho* substitutions such as **14f** and **14i** decreased potency relative to corresponding *meta* and *para* analogues. *Meta*-substituted analogues **14b** and **14h** demonstrated good potency against GT1b but were generally less inhibitory against GT2a. Similarly 3,4-disubstituted analogues, **14j** and **14k** in particular, were potent against GT1b but were significantly less potent against GT2a. *Para*-substituted analogues incorporating smaller groups (e.g., **14a**, **14d**, **14g**) showed promising potency against both GT1b and GT2a, whereas analogues with larger groups at this position could show a loss of activity (e.g., **14n** and **14o**). In addition to good potency, 14D showed promising pharmacokinetics and stability and was selected to undergo further studies as a lead compound. In Sprague–Dawley (S–D) rats at 10 mg kg^{-1}, a single dose had 45% bioavailability and an $AUC_{0-\infty}$ of 25.9 μM × h. In monitoring early clinical trials of other HCV non-nucleoside inhibitors NS5B in development at the time, however, fragility to viral resistance in vivo appeared to be a significant liability.[17–19] Thus it became clear that to develop a viable clinical candidate, dramatic enhancements in potency were required to ensure potency across the diverse genetic variability observed in chronic HCV patients including potential resistant variants.

All previous efforts to improve potency via modification of either the benzofuran C2 aryl group or the C3 methyl amide group were met with failure. Even simple alterations of the C3 amide, such as methylamide to ethyl amide, led to total loss of potency. The C2 aryl group tolerated modest changes but the 4-fluorophenyl analogues were consistently superior.

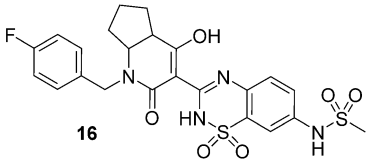

To determine the optimal direction required to improve the profile of new compounds, we re-examined the crystal structure of our original lead HCV-796[20], noting that the palm II binding site is located adjacent to the palm I binding site, and postulated that these regions could be contiguous. When modeling overlapping crystal structures of HCV-796 and the palm I thiadiazine **16**,[21] these binding pockets appeared contiguous (Figure 1) such that a suitably constructed molecule might interact with both pockets. This structure provided evidence that hybrid molecules may simultaneously interact with both pockets by addition of pendant groups attached to the C5 aryl ring.

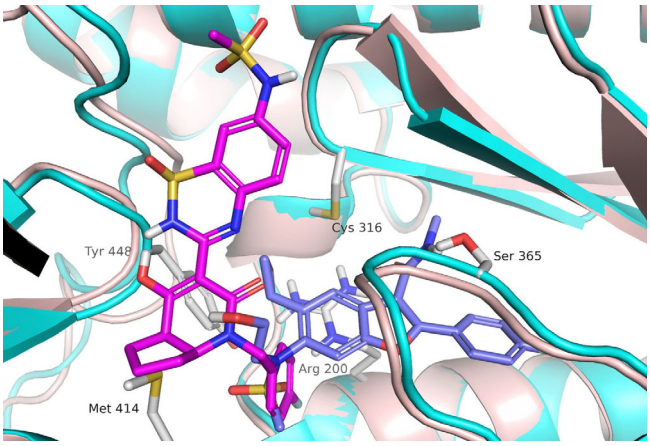

Figure 1. Overlay of HCV-796 and palm I thiadiazine inhibitor. HCV-796 located in the palm II binding site interacts with key serine 365 via the methyl amide at position 3 of the phenyl benzofuran core (lavender). Its partial overlap with the palm I thiadiazine compound (purple) is evident above arginine 200.

The initial approach toward accessing the palm I binding pocket used mono-substituted aryl groups to generate simple SAR and identify the best site and linker for introducing pendant groups. As shown earlier with compound **14o**, larger pendant groups could be introduced at the 4-postion while still maintaining some activity. Initially the potency was inferior to compounds with smaller substituents, but as larger groups as in **17a** were added the potency improved (Scheme 3).

This result provided the first evidence that an appropriately sized group could adopt a suitable binding orientation with the palm I region. Analogous to prior trends, introduction of larger pendant groups at the 2-position resulted in dramatic potency losses, and these analogues were abandoned. Finally, placing the pendant group at the 3-position of the aryl (**17b**) resulted in a significant boost in inherent activity and provided the most potent analogues generated to date. As additional analogues were synthesized and tested, it became clear that this was the favored position in all cases, with the results for an array of representative analogues shown in Table 3.

Diverse linkers to the pendant aryl groups were tolerated such as ethers (**17d**, **17h**), sulfones (**17f**, **17g**), amides (**17k**,

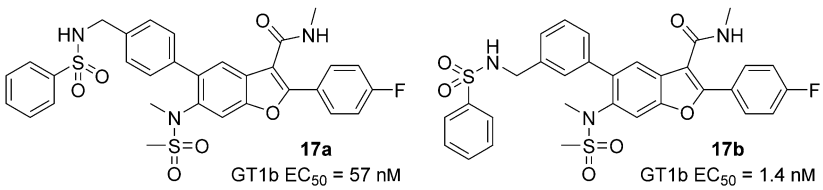

Scheme 3. Anti-HCV replicon activity of **17a** and **17b** with pendant linker.

Table 3. Anti-HCV replicon activity of compound **1a** analogues with pendant aryl groups.

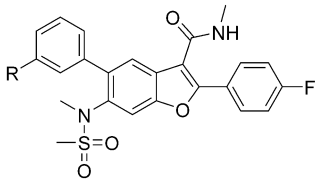

Compd	R	EC_{50} [nM][a] GT1b	GT2a	Compd	R	EC_{50} [nM][a] GT1b	GT2a
17c[b]		17	21	**17m**	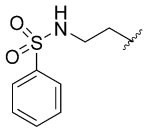	11	13
17d[b]		13	228	**17n**	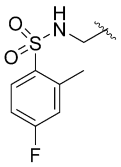	16	95
17e[b]	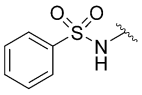	11	13	**17o**	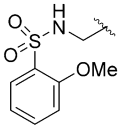	1	17
17f	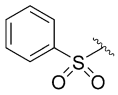	7	49	**17p**	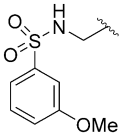	1	6
17g	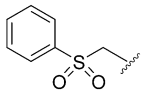	2	7	**17q**	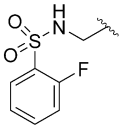	2	3
17h[b]	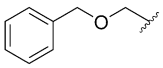	8	19	**17r**	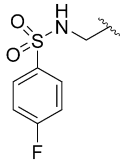	7	13
17i[b]	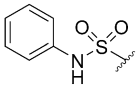	77	226	**17s**[b]	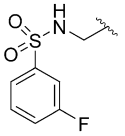	1	5
17j	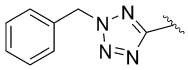	5	10				
17k	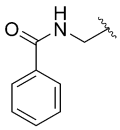	40	36				
17l[b]	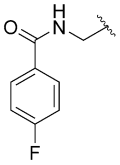	44	76				

[a] Data are the mean of $n \geq 2$ determinations unless otherwise noted. [b] $n = 1$.

17l), as well as heterocycles such as the tetrazole **17j**. Ultimately, sulfonamides linked through a benzylic amine or ethylamine (**17m**) emerged as highly potent analogues against both GT1b and GT2a. Extensive optimization led to inhibitors including **17p**, **17q**, and **17s** that possessed low single digit nanomolar potencies (EC_{50}) against both genotypes. Although these compounds were selected for further investigation, they consistently showed very poor PK profiles. Metabolite ID experiments showed the compounds underwent rapid degradation with the primary metabolic pathway being oxidation at the benzylic position. Attempts to make truncated sulfonamides lacking the benzylic methylene led to **17e** and **17i** but manifested in a loss of potency (10- to 100-fold).

An alternative strategy to protect the benzylic position from oxidation was to link it to the pendant aromatic ring to generate a fused aromatic heterocycle (Scheme 4). Initial compounds showed good potency, and more importantly attractive improvements in metabolic stability leading to promising pharmacokinetic profiles. Extensive optimization showed that a range of fused heterocycles was tolerated. However, the 5,6-fused heterocycles linked at the 2-position were consistently the most potent analogues (Table 4). Surveying unsubstituted

Table 4. Anti-HCV replicon activity of heterocyclic analogues.

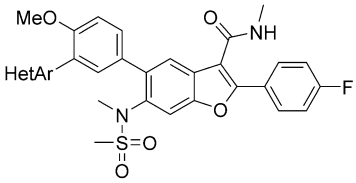

Compd	HetAr	EC_{50} [nM][a] GT1b	GT2a	Compd	HetAr	EC_{50} [nM][a] GT1b	GT2a
19a	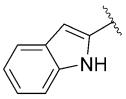	7	17	**19k**	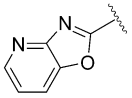	2	7
19b[b]	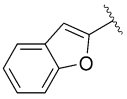	11	23	**19l**	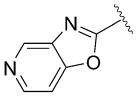	4[b]	9
19c[b]	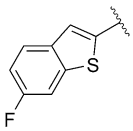	27	186	**19m**[b]		14	70
19d	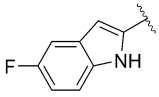	2	5	**19n**[b]	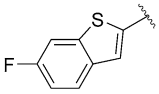	27	186
19f[b]	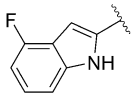	8	15	**19o**[b]	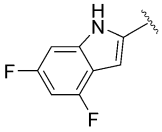	9	31
19g	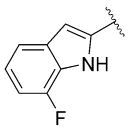	2	4	**19p**	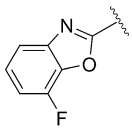	2	6
19h	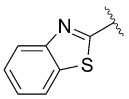	11	36	**19q**	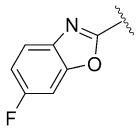	2	14
19i	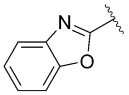	1	16[b]	**19r**	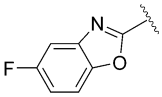	3	12
19j	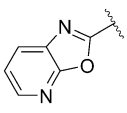	2	7	**20**	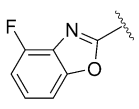	0.9	3

[a] Data are the mean of $n \geq 2$ determinations unless otherwise noted. [b] $n = 1$.

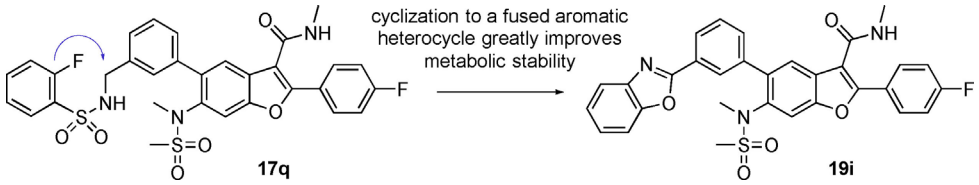

Scheme 4. Cyclization of aryl sulfonamide shields benzylic position from oxidation.

rings led to the finding that benzoxazoles and pyridyloxazoles such as **19l**, **19j**, and **19k** generally had the best potency. In addition, it was discovered that incorporation of a 4-methoxy substituent into the central phenyl ring removed activity in the hERG screening assay. As the compounds were further evaluated for properties such as permeability and pharmacokinetics, we found that incorporation of fluorine to the ring not only improved permeability and bioavailability, but also increased potency. Ultimately, 7-fluorobenzoxazole **20** was selected to be further evaluated as a lead candidate due to its overall profile.

Characterization of fluorobenzoxazole 20

Fluorobenzoxazole **20** underwent a detailed in vitro potency evaluation against both a genotype panel and a panel of common resistance mutations to palm-binding non-nucleoside inhibitors in the genotype 1 background (Table 5). Across this genotype panel **20** showed low nanomolar potency. There was approximately a 10-fold shift in 50% serum (data not shown). Compound **20** also retained its potency against well-characterized non-nucleoside inhibitor mutations in the GT1b background, although there was some attenuation of potency against similar mutations in the GT1a background.

Table 5. In vitro potency profile of fluorobenzoxazole **20**.

Genotype	EC_{50} [nM][a]	Mutant	EC_{50} [nM][a]
1a	2.7±2.0	**1b** C316Y	9.2±5.5
1b	3.1±1.0	**1b** M414V	5.1±3.4
2a	25.4±16.9	**1a** C316Y	123.9±86.1
2b	9.1±2.3	**1a** S365A	197±107
3a	3.3±2.2		
4a	3.0±1.7		

[a] Values are the average of $n \geq 3$ determinations.

The pharmacokinetic properties of **20** were characterized using Sprague–Dawley rats and beagle dogs (Table 6). Fluorobenzoxazole **20** showed modest bioavailability, exposure, moderate clearance, and C_{24h} drug concentrations well above the serum adjusted GT1a or 1b EC_{50} values in both species. In general, the modest bioavailability was due to the poor solubility of **20**. Evaluated in the context of its in vitro potencies, however, these parameters suggested that **20** would demonstrate efficacy in an in vivo model of chronic HCV infection. To prepare for an efficacy proof-of-concept study in chronic HCV-infected chimpanzees, **20** was orally dosed as a suspension in Tang to two uninfected chimpanzees at a dose of 5 mg kg^{-1} (Table 6). Fluorobenzoxazole **20** achieved good exposure and a low-micromolar C_{max}. Although sufficient sampling to determine clearance was not possible, the mean plasma concentration at 12 h was 0.71 μM, well above the serum-adjusted EC_{50} for genotype 1. Based on this acceptable profile, **20** was advanced to an in vivo efficacy study in chronic HCV-infected chimpanzees.

Fluorobenzoxazole **20** was dosed to two high viral load (VL) chronic HCV-infected chimpanzees (GT1a, VL 5.73 log IU mL^{-1}; GT1b, VL 6.13 log IU mL^{-1}) at 2 mg per kg body weight (≈120 mg) q.d. for seven days (Figure 2). Both animals experienced ≈2 log decrease in viral load by the end of the dosing interval, with a modest rise in viremia by the end of an additional week post-dosing. Viral load was at its nadir at the end of dosing, with plasma drug concentrations 24 h after the final dose of 0.5 μM (GT1a) and 1.2 μM (GT1b), approximately 570- and 175-fold above the serum-adjusted EC_{50} values. Baseline and end-of-dosing samples were sequenced to evaluate emergence of resistance; there was no evidence for either emerging resistance or enhanced populations of pre-existing viral var-

Table 6. Pharmacokinetic parameters of fluorobenzoxazole **20**.

Parameter	S–D Rat ($n=2$)	Beagle Dog ($n=2$)	Chimpanzee ($n=2$)
Dose i.v. [mg kg^{-1}]	2	1	
CL [mL min^{-1} kg^{-1}]	2.0±0.5	2.3±1.4	
$t_{1/2}$ [h]	3.8±1.4	27.2±14.3	
Dose p.o. [mg kg^{-1}]	10	5	5
C_{max} [μM]	3.7±1.4	0.5±0.1	1.2±0.2
t_{max} [h]	5.0±1.0	4.0±0.0	6.0±2.0
$AUC_{0-\infty}$ [μM×h]	29.9±11.6	6.6±0.9	25.6±12.1
F [%]	21.8±8.5	14.2±1.1	ND[a]
C_{24h} [μM]	0.110±0.11	0.10±0.02	C_{12h}: 0.71±0.20

[a] Not determined.

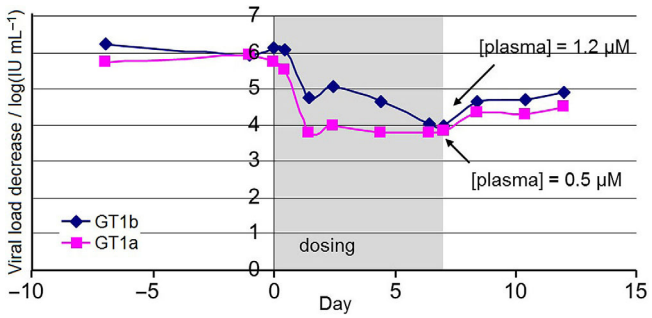

Figure 2. Fluorobenzoxazole **20** in vivo efficacy study. Fluorobenzoxazole **20** was dosed at 2 mg kg^{-1} (≈120 mg) once daily for seven days as a suspension in Tang to two chronic HCV-infected chimpanzees harboring GT1a or GT1b infections. Blood samples were collected periodically, processed to plasma, and evaluated for HCV viral load. Plasma drug concentrations 24 h following completion of dosing are shown.

iants in samples collected 24 h following the final dose, when viremia was at its most suppressed. Of note, the results against the GT1a infection were every bit as robust as those against the GT1b infection. However, the in vitro potency losses against some mutants in the GT1a background with **20** compelled us to seek a superior analogue for clinical development.

Discovery of MK-8876

Concurrent with the evaluation of **20**, continued optimization of the pendant heterocycle moiety was conducted to improve potency against mutations in the GT1a background. During an exploration of the impact of introducing ring constraints, we learned that formation of the tetracycles shown in Table 7 generated analogues with exceptional potency. Likely due to the ring constraint, these compounds were sensitive to the substitution pattern around the ring. For example, tetracycles with a substitution at the 6- or 7-position of the indole ring such as **22i** and **22j** lost potency against GT2a. In contrast, a substitution at the 4- or 5-position of the indole such as **22k** and **23** maintained or improved potency against all genotypes tested. In addition, these tetracycles showed excellent chemical and metabolic stability as well as good pharmacokinetic profiles. Tetracycle **23** in particular possessed excellent potency when tested against a broad genotype and mutant panel. Based on these early assessments, this compound was selected for advancement and underwent a full characterization, ultimately becoming the clinical candidate MK-8876.

Characterization of MK-8876

The in vitro potency of MK-8876 (**23**) was determined against a broad replicon panel of HCV genotypes and NS5B non-nucleoside mutants (Table 8). Overall, MK-8876 displayed excellent potency across the panel, having a nearly equipotent profile in the low single digit nanomolar range across the spectrum. Significantly, the potency profile of MK-8876 against the clinically relevant NS5B non-nucleoside mutants showed the greatest differentiation from its predecessor **20**. MK-8876 retained its potency across all mutants tested with no significant loss in activity observed. The difference in potency of MK-8876 was particularly significant against the C316Y and S365A mutants and even more so against the 1a C316Y:C445F double mutant.

The pharmacokinetics of MK-8876 (**23**) were profiled in Sprague-Dawley rats and beagle dogs (Table 9). In Sprague-Dawley rats MK-8876 showed moderate clearance and a half-life of 6.1 h. A 10 mg kg^{-1} oral dose in S–D rats gave a C_{max} of 1.12 μM and a tmax of 7 h with 35% bioavailability. In the beagle dog MK-8876 showed low clearance and a half-life of 4.9 h. A 5 mg kg^{-1} oral dose in beagle dogs gave a C_{max} of 1.2 μM and a tmax of 1.2 h with 26% bioavailability. The C_{24h} plasma drug concentrations were 0.169 μM (rat) and 0.102 μM (dog), both well above the serum-adjusted EC_{50} values of the replicon panel. The results were consistent with the profile of a compound suitable for once daily dosing which was essential for a lead compound that was intended to be dosed as part of combination therapy.

Finally, we obtained a crystal structure of MK-8876 (**23**) bound to the GT1b NS5B polymerase (Figure 3). As originally postulated, the 2-phenylbenzofuran region of the molecule interacted within the palm II binding site, as previously known for compounds with similar core structures (e.g., HCV-796). Importantly, the methyl amide at position 3 of the 2-phenylbenzofuran engages in key interactions with serine 365 but does not interact with residue 316. We note that the crystal structure was obtained for the GT1b BK form of NS5B, which naturally encodes an asparagine at residue 316 rather than the more common cysteine. The tetracyclic region of MK-8876 filled the hydrophobic palm I binding site, flanking the methionine 414 and tyrosine 448 residues. This crystal structure clearly confirmed that palm I and palm II sites were and could be simultaneously bound, leading to a significant improvement in potency versus molecules without this capability. This improvement in potency is particularly evident in the case of NS5B mutants. The specific interactions at the residue level that are the

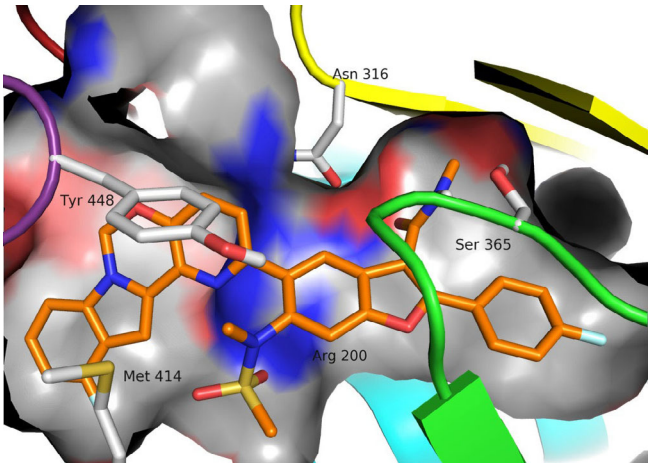

Figure 3. MK-8876 (**23**) crystal structure bound to GT1b NS5B polymerase. The phenylbenzofuran core binds to the palm II site, projecting methyl amide at position 3 and sulfonamide at position 6 critical for ligand potency. The tetracyclic substituent at position 5 extends to the hydrophobic palm I site.

Table 7. Anti-HCV replicon activity of fused heterocyclic analogues.

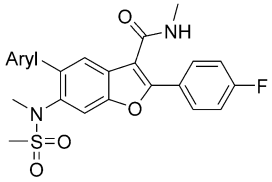

Compd	Aryl	EC_{50} [nM][a] GT1b	GT2a	Compd	Aryl	EC_{50} [nM][a] GT1b	GT2a
22a	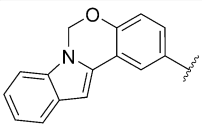	2	6	**22i**[b]	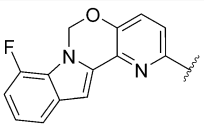	7	39
22b	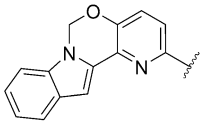	5	11	**22j**[b]	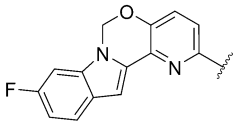	4	24
22c[b]	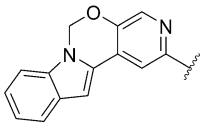	2	18	**22k**	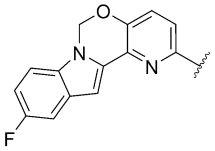	4	3
22d[b]	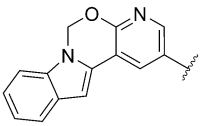	5	14	**23**	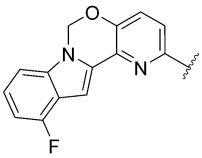	3	2
22e[b]	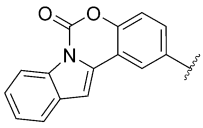	8	17	**23a**	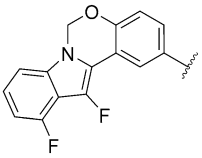	4	4
22f	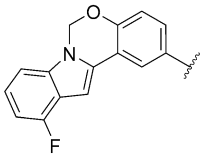	4	4	**23b**	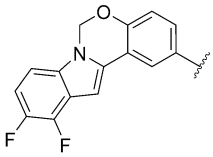	5	3
22g	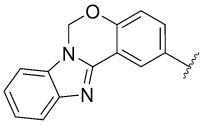	3	7	**23d**	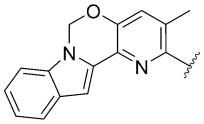	19	13
22h	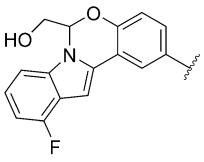	3	4	**23f**	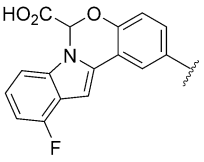	23	27

[a] Data are the mean of $n \geq 2$ determinations unless otherwise noted. [b] $n = 1$.

basis of this potency improvement could not been determined. However, it is clear that the tetracyclic motif of MK-8876 results in palm I binding site induced fit associated with large dispersion interactions resulting in the observed potency boost. In addition, the absence of specific polar interactions with amino acids at key positions is an advantage for pan-genotypic potency and mutant resistance.

Table 8. In vitro potency profile of MK-8876 (**23**).

Genotype	EC_{50} [nM][a]	Mutant	EC_{50} [nM][a]
1a	1.6 ± 1.2	**1b** C316Y	2.7 ± 2.2
1b	2.2 ± 0.7	**1b** S365A	1.1 ± 0.3
2a	7.3 ± 5.2	**1b** M414I	4.0 ± 2.1
2b	3.9 ± 2.1	**1b** M414T	1.8 ± 0.9
3a	1.8 ± 1.1	**1b** M414V	1.3 ± 0.7
4a	1.2 ± 0.7	**1a** C316Y	2.3 ± 0.9
5a	1.2 ± 0.7	**1a** S365A	1.0 ± 0.6
		1a S365T	6.6 ± 1.6
		1a M414I	2.0 ± 0.8
		1a M414V	2.0 ± 0.7
		1a C316Y:C445F	3.2 ± 1.5

[a] Values are the average of $n \geq 3$ determinations.

Table 9. Pharmacokinetic parameters of MK-8876 (**23**).

Parameter	S–D Rat ($n = 2$)	Beagle Dog ($n = 3$)
Dose i.v. [mg kg^{-1}]	2	1
CL [mL min^{-1} kg^{-1}]	7.3 ± 2.0	3.0 ± 0.5
$t_{1/2}$ [h]	6.1 ± 1.2	9.2 ± 0.3
Dose p.o. [mg kg^{-1}]	10	5
C_{max} [μM]	1.1 ± 0.3	1.2 ± 0.8
t_{max} [h]	7.0 ± 1.0	1.2 ± 0.8
$AUC_{0-\infty}$ [μM × h]	13.5 ± 2.3	12.2 ± 4.4
F [%]	35.3 ± 5.9	24.7 ± 6.4
C_{24h} [μM]	0.169 ± 0.001	0.102 ± 0.018

Conclusions

A research program directed at developing a non-nucleoside inhibitor of HCV NS5B based on the benzofuran core of HCV-796 led to the discovery of a novel structural class of 5-aryl benzofurans that interact with both the palm I and palm II binding regions. An extensive medicinal chemistry effort resulted in the identification of a series of pendant heterocycles suitable for further development, most notably the fluorobenzoxazole **20**, although subsequent characterization of **20** identified deficiencies against clinically relevant resistance variants. Further optimization of the pendant heterocycle through incorporation of a ring constraint successfully led to the discovery of MK-8876 (**23**). MK-8876 demonstrated a broadly acting genotypic potency profile and improved potency against clinically relevant mutants. In addition, MK-8876 showed a good preclinical pharmacokinetic profile indicating it would be suitable for once daily dosing. MK-8876 has successfully completed Phase 1 monotherapy studies for evaluation and characterization as a future component of an all-oral direct-acting regimen for the treatment of HCV.

Experimental Section

Chemistry

Commercially available reagents, solvents, and intermediates were used as received unless otherwise noted. Other reagents and intermediates were prepared as described. ^{1}H NMR spectra were obtained on a Varian VNMR System 400 (400 MHz) and are reported as ppm downfield from TMS. The synthetic procedures of individual analogues were carried out using described procedures.[16] The optimized synthesis of MK-8876 (compound **23**) was developed in the MSD Process Laboratories and reported previously.[22]

Procedure for the synthesis of compound 20

Step 1: 1-fluoro-3-methoxy-2-nitrobenzene: To a 0 °C solution of 1,3-difluoro-2-nitrobenzene (100 g, 0.63 mol) in MeOH (1.3 L) was slowly added a solution of MeONa (0.69 mol in MeOH, freshly prepared from 15.9 g of sodium metal and 200 mL of MeOH). The resulting reaction was allowed to stir for about 15 h at room temperature, then the reaction mixture was concentrated and diluted with EtOAc. The organic phase was washed sequentially with water and brine, dried over Na_2SO_4, then filtered and concentrated in vacuo to provide 1-fluoro-3-methoxy-2-nitrobenzene (98 g, 91% yield) which was used in the next step without further purification. ^{1}H NMR ($CDCl_3$, 400 MHz) δ = 7.38–7.44 (m, 1H), 6.72–6.88 (m, 2H), 3.95 ppm (s, 3H).

Step 2: 3-fluoro-2-nitrophenol: To a −40 °C solution of 1-fluoro-3-methoxy-2-nitrobenzene (98 g, 0.57 mol) in dichloromethane (500 mL) was added dropwise a solution of BBr_3 (1 L, 1 M in dichloromethane). The resulting reaction was allowed to stir for about 15 h at room temperature then the reaction mixture was slowly poured into ice water (500 mL). The resulting solution was extracted with EtOAc and the combined organic layers were washed with 5% aqueous $NaHCO_3$, brine, and then dried over Na_2SO_4. The mixture was filtered and concentrated to provide 3-fluoro-2-nitrophenol (85 g, 95% yield) which was used in the next step without further purification. ^{1}H NMR ($CDCl_3$, 400 MHz) δ = 7.43–7.49 (m, 1H), 6.88 (d, J = 8.0 Hz, 1H) 6.73–6.78 ppm (m, 1H).

Step 3: 2-amino-3-fluorophenol: 3-fluoro-2-nitrophenol (38 g, 0.24 mol) was dissolved in EtOH and then palladium on carbon (5 g, 10% Pd) was added. The reaction flask was evacuated and the reaction mixture was stirred under an H_2 atmosphere (1 atm) for 3 h at room temperature. The reaction mixture was then filtered through a short pad of Celite and washed through with EtOH. The combined filtrate was concentrated to provide 2-amino-3-fluorophenol (26 g, 86% yield) which was used in the next step without further purification. ^{1}H NMR ($CDCl_3$, 400 MHz) δ = 9.43 (s, 1H), 6.42–6.53 (m, 2H), 6.32–6.42 (m, 1H), 4.34 ppm (s, 2H).

Step 4: 2-(5-bromo-2-methoxyphenyl)-4-fluorobenzo[d]oxazole: To a solution of 2-amino-3-fluorophenol (9 g, 70.8 mmol) in 10 mL of PPA was added 5-bromo-2-methoxybenzoic acid (16.3 g, 70.8 mmol) and the resulting mixture was heated at 140 °C and stirred for 4 h. The reaction mixture was then poured into ice water (50 mL) and extracted with EtOAc. The organic extract was concentrated and the residue was purified via flash chromatography on silica gel (petroleum ether/ethyl acetate 10:1) to provide 2-(5-bromo-2-methoxyphenyl)-4-fluorobenzo[*d*]oxazole (16 g, 82% yield) as a solid. ^{1}H NMR ($CDCl_3$, 400 MHz) δ = 8.29 (d, J = 2.4 Hz, 1H), 7.57–7.54 (m, 1H), 7.40 (d, J = 8.0 Hz, 1H), 7.27–7.33 (m, 1H), 7.07 (m, 1H), 6.96 (d, J = 9.2 Hz, 1H), 3.99 ppm (s, 3H).

Step 5: 4-fluoro-2-(2-methoxy-5-(4,4,5,5-tetramethyl-1,3,2-dioxaborolan-2-yl)phenyl)benzo[d]oxazole: A solution of 2-(5-bromo-2-methoxyphenyl)-4-fluorobenzo[*d*]oxazole (18.4 g, 57.1 mmol) and bis(pinacolato)diboron (17.4 g, 68.5 mmol) in DMF (10 mL) was stirred under a nitrogen atmosphere. Pd(dppf)Cl_2 (500 mg) and potassium acetate (10 g, 114 mmol) were added. The mixture was

heated at 80 °C and stirred for 3 h. The reaction mixture was then cooled and concentrated in vacuo. The residue was dissolved in dichloromethane and filtered through a pad of Celite. The solution was washed with H_2O, brine, dried over Na_2SO_4 then filtered and concentrated. The residue was purified by flash chromatography on silica gel (petroleum ether/ethyl acetate 10:1) to provide 4-fluoro-2-(2-methoxy-5-(4,4,5,5-tetramethyl-1,3,2-dioxaborolan-2-yl)-phenyl)benzo[d]oxazole (10 g, 54% yield) as a solid. ^{1}H NMR ($CDCl_3$, 400 MHz) $\delta = 8.53$ (d, $J = 1.6$ Hz, 1H), 7.85–7.92 (m, 1H), 7.44 d, $J = 8.0$ Hz, 1H), 7.20–7.28 (m, 1H), 6.96–7.05 (m, 2H), 3.97 (s, 3H), 1.29 ppm (s, 12H).

Step 6: 5-(3-(4-fluorobenzo[*d*]oxazol-2-yl)-4-methoxyphenyl)-2-(4-fluorophenyl)-*N*-(methyl-6-(*N*-methylsulfonamido)benzofuran-3-carboxamide (compound 20): To a solution of bromide **13** (5 g, 11.0 mmol) and 4-fluoro-2-(2-methoxy-5-(4,4,5,5-tetramethyl-1,3,2-dioxaborolan-2-yl)phenyl)benzo[*d*]oxazole (5.27 g, 14.3 mmol) in DMF (150 mL) under nitrogen was added Pd(dppf)Cl_2 (200 mg) and K_3PO_4 (4.66 g, 22.0 mmol). The reaction mixture was heated at 100 °C and allowed to stir for 10 h then cooled and concentrated in vacuo. The residue was dissolved in dichloromethane and filtered through a pad of Celite. The filtrate was washed sequentially with water and brine then dried over Na_2SO_4, filtered and concentrated. The crude product was purified by flash chromatography on silica gel (petroleum ether/ethyl acetate 5:1) to provide 5-(3-(4-fluorobenzo[*d*]oxazol-2-yl)-4-methoxyphenyl)-2-(4-fluorophenyl)-*N*-(methyl-6-(*N*-methylsulfonamido)benzofuran-3-carboxamide (compound 20)(3.8 g, 56% yield) as a white solid. ^{1}H NMR ($CDCl_3$, 400 MHz) $\delta = 8.21$ (d, $J = 2.0$ Hz, 1H), 7.91–7.95 (m, 2H), 7.83 (s, 1H), 7.68 (d, $J = 2.0$ Hz, 1H), 7.66 (s, 1H), 7.39 (d, $J = 8.0$ Hz, 1H), 7.14–7.27 (m, 4H), 7.06 (t, $J = 8.4$ Hz, 1H), 5.95 (br s, 1H), 4.06 (s, 3H), 3.14 (s, 3H), 2.99 (d, $J = 4.8$ Hz 3H), 2.77 ppm (s, 3H); MS $(M+H)^+$ 618.

Crystallography

Crystals of HCV NS5B(1b/BK)Δ21 were prepared as previously described.[23] Once grown, crystals were soaked for three days in reservoir solution supplemented with 1 mM MK-8876, then cryoprotected and flash-cooled as described. Diffraction data were collected on a Dectris PILATUS 6 M detector installed at IMCA-CAT beamline 17-ID at the Advanced Photon Source. Data were processed using autoPROC[24], and TLS refinement was conducted using autoBUSTER[25] and Coot[26] with HCV NS5B(1b/BK)Δ21 apoprotein (PDB ID: 1C2P) as a starting model. Data collection and refinement statistics are listed in Table 10. The structure of the HCV NS5B complex with MK-8876 has been deposited at the PDB with accession code 5W2E.

Computational chemistry and modeling studies

Crystal structures were used as starting point for modeling work executed using MOE (Molecular Operating Environment, version 2013.08; Chemical Computing Group Inc., 1010 Sherbooke St. West, Suite #910, Montreal, QC, H3A 2R7 (Canada), 2017). Protein preparation was applied to the initial structures and coordinates were refined with harmonic constraints using the MMFF94x force-field. Ligand minimization was performed using the MMFF94x force-field with either rigid or flexible protein residues in the binding sites (up to 6 Å radius around the bound ligand).

Table 10. Data collection and refinement statistics.

Parameter	Value
Wavelength [Å]	1.000
Frame width [°]/Total sweep [°]	0.25/180
Space group	$P2_12_12_1$
Cell dimensions	
a, *b*, *c* [Å]	86.1, 106.4, 126.1
α, β, γ [°]	90, 90, 90
Resolution [Å][a]	126–2.80 (2.95–2.80)
R_{merge}[a]	0.149 (0.667)
$I/\sigma(I)$[a]	10.1 (2.7)
Completeness [%][a]	100 (99.9)
Redundancy[a]	6.6 (6.8)
Refinement	
Resolution [Å]	2.8
Reflections	29173
R_{work}/R_{free}	0.18/0.24
No. non-hydrogen atoms	
Protein	8715
Waters	259
Ligands	88
***B*-factors (average) [Å^2]**	
Protein	46
Waters	34
Ligands	54
RMSD bonds [Å]/angles [°]	0.010/1.14

[a] Highest-resolution shell shown in parentheses.

Biology

All animal studies were performed according to the NIH Guide for the Care and Use of Laboratory Animals, and experimental protocols were approved by the Institutional Animal Care and Use Committees of Merck & Co., Inc., Kenilworth, NJ USA. The HCV genotype was determined by a line probe assay (Versant HCV genotype assay, LiPa, Bayer Diagnostics/Innogenetics) and confirmed by RT-PCR rescue and sequencing of HCV genetic material.[27] HCV-infected chimpanzees were dosed orally at 5 mg kg^{-1} for a single dose or q.d. for seven days at 2 mg kg^{-1} by the voluntary ingestion of compound **20** (in a Tang vehicle). Viral load determinations were performed on plasma samples using the HCV TaqMan assay (Cenetron Diagnostics, Austin, TX). Viral resistance analysis of chimpanzee plasma samples was conducted similarly to a previously published protocol using NS5B specific primers.[27] Initial potency screening was conducted against GT1b or GT2a replicon cell lines using a luciferase-based reporter assay.[28] The assay was automated which enabled rapid screening of many compounds; however, the assay required robust expression of a co-encoded luciferase gene which in practice restricted its use to very few genotypes. For compounds of greater interest, additional and more rigorous EC_{50} determinations were generated against broad panels of genotype and mutant replicon cell lines, and were conducted using a sensitive but lower through-put TaqMan based assay.[29] Potency values reported from the TaqMan assay may vary slightly from those generated with the luciferase-based reporter assay due to differences in cell lines and assay conditions. The NS5B sequences for the genotypes are GT1a H77 (GenBank AJ238799), GT1b con1 (GenBank AB047639), GT2a JFH (GenBank AB047639), GT2b (GenBank D10988), GT3a (GenBank 17763), and GT4a,[30] and GT5a (Gen-

Bank 009826). Inhibitors from this study typically were modest at best in potency when using an NS5B enzymatic assay. The data enabled poor discrimination among compounds, and its use was abandoned early in the program.

Pharmacokinetic studies

Studies were performed in both rats and dogs. The study protocols were reviewed and approved by the Institutional Animal Care and Use Committees at Merck & Co., Inc., Kenilworth, NJ USA. For studies in which compound **20** was dosed intravenously to rats or dogs, compound was formulated in DMSO and administered as a bolus at 2 mg kg^{-1} (male Sprague–Dawley rat) or formulated in 10% EtOH 70% polyethylene glycol 400 (PEG400) and administered at 1.0 mg kg^{-1} (male Beagle dog). For oral studies, compound **20** was dosed in PEG 400 at 10 mg kg^{-1} as a suspension (rat) or at 5 mg kg^{-1} as a solution (dog). For studies in which MK-8876 was dosed intravenously to rats or dogs, compound was formulated in DMSO and administered as a bolus at 2 mg kg^{-1} (male Sprague–Dawley rat) or formulated in DMSO/PEG400/water at a 2:6:2 ratio and administered as a bolus at 1 mg kg^{-1} (male beagle dog). For oral studies MK-8876 was dosed as a suspension in PEG 400 at 10 mg kg^{-1} (rat) or as a suspension in 0.5% methylcellulose/0.25% sodium dodecyl sulfate/5 mM HCl at 5 mg kg^{-1} (dog). For all studies, blood samples were collected in EDTA-containing tubes at appropriate times, plasma separated by centrifugation and stored at −70 °C until analysis. Quantitation of compound 20 or MK-8876 levels was conducted by high performance liquid chromatography/tandem mass spectrometry (LC–MS/MS), following protein precipitation.

Conflict of interest

The authors declare no conflict of interest.

Keywords: hepatitis C · inhibitors · MK-8876 · non-nucleoside · NS5B

[1] D. Lavanchy, *Clin. Microbiol. Infect.* **2011**, *17*, 107 – 115.
[2] R. S. Brown, *Nature* **2005**, *436*, 973 – 978.
[3] P. Ferenci, D. Bernstein, J. Lalezari, D. Cohen, Y. Luo, C. Cooper, E. Tam, R. T. Marinho, T. Naoky, A. Nyberg, T. D. Box, Z. Younes, P. Enayati, S. Green, Y. Baruch, B. R. Bhandari, F. A. Caruntu, T. Sepe, V. Chulanov, E. Janczewska, G. Rizzardini, J. Gervain, R. Planas, C. Moreno, T. Hassanein, W. Xie, M. King, T. Podsadecki, K. R. Reddy, *N. Engl. J. Med.* **2014**, *370*, 1983 – 1992.
[4] K. V. Kowdley, S. L. Gordon, K. R. Reddy, L. Rossaro, D. E. Bernstein, E. Lawitz, M. L. Shiffman, E. Schiff, R. Ghalib, M. Ryan, V. Rustgi, M. Chojkier, R. Herring, A. M. Di Bisceglie, P. J. Pockros, G. M. Subramanian, D. An, E. Svarovskaia, R. H. Hyland, D. Phil, P. S. Pang, W. T. Symonds, J. G. McHutchison, A. J. Muir, D. Pound, M. W. Fried, *N. Engl. J. Med.* **2014**, *370*, 1973 – 1982.
[5] S. Zeuzem, R. Ghalib, K. R. Reddy, P. J. Pockros, Z. B. Ari, Y. Zhao, D. D. Brown, S. Wan, M. J. DiNubile, B. Y. Nguyen, M. N. Robertson, J. Wahl, E. Barr, J. R. Butterton, *Ann. Intern. Med.* **2015**, *163*, 1 – 13.
[6] R. Bartenschlager, F. L. Cosset, V. Lohmann, *J. Hepatol.* **2010**, *53*, 583 – 585.
[7] D. B. Smith, J. Bukh, C. Kuiken, A. S. Muerhoff, C. M. Rice, J. T. Stapleton, P. Simmonds, *Hepatology* **2014**, *59*, 318 – 327.
[8] S. S. Carroll, D. B. Olsen, *Infect. Disord. Drug Targets* **2006**, *6*, 17 – 29.
[9] L. Gerber, T. M. Welzel, S. Zeuzem, *Liver Int.* **2013**, *33*, 85 – 92.
[10] C. Caillet-Saguy, P. C. Simister, S. Bressanelli, *J. Mol. Biol.* **2011**, *414*, 370 – 384.
[11] G. T. Everson, K. D. Sims, P. J. Thuluvath, E. Lawitiz, T. Hassanein, M. Rodriguez-Torres, T. Desta, T. Hawkins, J. M. Levin, F. Hinestrosa, V. Rustgi, H. Schwartz, Z. Younossi, L. Webster, N. Gitlin, T. Eley, S. P. Huang, F. McPhee, D. M. Grasela, P. F. Gardiner, *Liver. Int.* **2016**, *36*, 189 – 197.
[12] N. M. Kneteman, A. Y. Howe, T. Gao, J. Lewis, D. Pavear, G. Lund, D. Douglas, D. F. Mercer, D. L. Tyrrell, F. Immermann, I. Chaudhary, J. Speth, S. A. Villano, J. O'Connell, M. Collett, *Hepatology* **2009**, *49*, 745 – 752.
[13] A. Maynard, R. M. Crosby, B. Ellis, R. Hamatake, Z. Hong, B. A. Johns, K. M. Kahler, C. Koble, A. Leivers, M. R. Leivers, A. Mathis, A. J. Peat, J. J. Pouliot, C. C. Roberts, V. Samano, R. M. Schmidt, G. K. Smith, A. Spaltenstein, E. L. Stewart, P. Thommes, E. M. Turner, C. Voitenleitner, J. T. Walker, G. Waitt, J. Weatherhead, K. Weaver, S. Williams, L. Wright, Z. Z. Xiong, D. Haigh, J. B. Shotwell, *J. Med. Chem.* **2014**, *57*, 1902 – 1913.
[14] K.-S. Yeung, B. R. Beno, K. Parcella, J. A. Bender, K. A. Grant-Young, A. Nickel, P. Gunaga, P. Anjanappa, R. O. Bora, K. Selvakumar, K. Rigat, Y.-K. Wang, M. Liu, J. Lemm, K. Mosure, S. Sheriff, C. Wan, M. Witmer, K. Kish, U. Hanumegowda, X. Zhuo, Y.-Z. Shu, D. Parker, R. Haskell, A. Ng, Q. Gao, E. Colston, J. Raybon, D. M. Grasela, K. Santone, M. Gao, N. A. Meanwell, M. Sinz, M. G. Soars, J. O. Knipe, S. B. Roberts, J. F. Kadow, *J. Med. Chem.* **2017**, *60*, 4369 – 4385.
[15] C. J. Burns, A. M. Del Vecchio, T. R. Bailey, B. A. Kulkami, T. H. Faitg, S. R. Sherk, C. W. Blackledge, D. J. Rys, T. A. Lessen, J Swestock, Y. Deng, T. J. Nitz, J. A. Reinhardt, H. Feng, A. K. Saha, (Viropharma Incorporated, Exton, USA, Wyeth, Madison, USA), Int. PCT Pub. No. WO2004041201, **2004**.
[16] C. C. McComas, N. J. Liverton, J. Habermann, U. Koch, F. Narjes, P. Li, X. Peng, R. Soll, H. Wu, (Merck Sharpe & Dohme Corp., Rahway, USA), Int. PCT Appl. No. WO2013033901 A1, **2013**; C. C. McComas, N. J. Liverton, J. Habermann, U. Koch, F. Narjes, P. Li, X. Peng, R. Soll, H. Wu, A. Palani, S. He, D. Xing, H. Liu, Z. Lai, C. London, D. Xiao, N. Zorn, R. P. Nargund, (Merck Sharpe & Dohme Corp., Rahway, USA), Int. PCT Appl. No. WO2013034048 A1, **2013**; C. C. McComas, N. J. Liverton, J. Habermann, U. Koch, F. Narjes, P. Li, X. Peng, R. Soll, H. Wu, A. Palani, S. He, D. Xing, H. Liu, Z. Lai, C. London, D. Xiao, N. Zorn, R. P. Nargund, (Merck Sharpe & Dohme Corp., Rahway, USA), Int. PCT Appl. No. WO2013034047 A1, **2013**; C. C. McComas, N. J. Liverton, J. Habermann, U. Koch, F. Narjes, P. Li, X. Peng, R. Soll, H. Wu, (Merck Sharpe & Dohme Corp., Rahway, USA) Int. PCT Appl. No. WO2013033900 A1, **2013**; C. C. McComas, N. J. Liverton, R. Soll, P. Li, X. Peng, H. Wu, F. Narjes, J. Habermann, U. Koch, S. Liu, (Merck Sharpe & Dohme Corp., Rahway, USA), Int. PCT Appl. No. WO2011106992A1, **2011**; C. C. McComas, N. J. Liverton, J. Habermann, U. Koch, F. Narjes, P. Li, X. Peng, R. Soll, H. Wu, (Merck Sharpe & Dohme Corp., Rahway, USA), Int. PCT Appl. No. WO2011106929 A1, **2011**; C. C. McComas, N. J. Liverton, R. Soll, P. Li, X. Peng, H. Wu, (Merck Sharpe & Dohme Corp., Rahway, USA), Int. PCT Appl. No. WO2011106986 A1, **2011**.
[17] P. Krishnan, R. Tripathi, G. Schnell, T. Reisch, J. Beyer, M. Irvin, W. Xie, L. Larsen, D. Cohen, T. Podsadecki, T. Pilot-Matias, C. Collins, *Antimicrob. Agents Chemother.* **2015**, *59*, 5445 – 5454.
[18] H. Mo, C. Hedskog, E. Svarovskaia, S.-C. Sun, I. M. Jacobson, D. M. Brainard, J. G. McHutchison, M. D. Miller, *J. Med. Virol.* **2016**, *23*, 644 – 651.
[19] P. J. F. Troke, M. Lewis, P. Simpson, K. Gore, J. Hammond, C. Craig, M. Westby, *Antimicrob. Agents Chemother.* **2012**, *56*, 1331 – 1341.
[20] J. Q. Hang, Y. Yang, S. F. Harris, V. Leveque, H. J. Whittington, S. Rajyaguru, G. Ao-leong, M. F. McCown, A. Wong, A. M. Giannetti, S. Le Pogam, F. Talamas, N. Cammack, I. Najera, K. Klumpp, *J. Biol. Chem.* **2009**, *284*, 15517 – 15529.
[21] F. Ruebsam, D. E. Murphy, C. V. Tran, L. S. Li, J. Zhao, P. S. Dragovich, H. M. McGuire, A. X. Xiang, Z. Sun, B. K. Ayida, J. K. Blazel, S. H. Kim, Y. Zhou, Q. Han, C. R. Kissinger, S. E. Webber, R. E. Showalter, A. M. Shah, M. Tsan, R. A. Patel, P. A. Thompson, L. A. Lebrun, H. J. Hou, R. Kamran, M. V. Sergeeva, D. M. Bartkowski, T. G. Nolan, D. A. Norris, J. Khandurina, J. Brooks, E. Okamoto, L. Kirkovsky, *Bioorg. Med. Chem. Lett.* **2009**, *19*, 6404 – 6412.
[22] M. J. Williams, Q. Chen, L. Codan, R. K. Dermenjian, S. Dreher, A. W. Gibson, H. Xianliang, Y. Jin, S. P. Keen, A. Y. Lee, D. R. Lieberman, W. Lin, G. Liu, M. McLaughlin, M. Reibarkh, J. P. Scott, S. Strickfuss, L. Tan, R. J. Varsolona, F. Wen, *Org. Process Res. Dev.* **2016**, *20*, 1227 – 1238.
[23] C. A. Lesburg, M. B. Cable, E. Ferrari, Z. Hong, A. F. Mannarino, P. C. Weber, *Nat. Struct. Biol.* **1999**, *6*, 937 – 943.

[24] C. Vonrhein, C. Fiensburg, P. Keller, A. Sharff, O. Smart, W. Paciorek, T. Womack, G. Bricogne, *Acta Crystallogr. Sect. D* **2011**, *67*, 293 – 302.
[25] G. Bricogne, E. Blanc, M. Brandl, C. Flensburg, P. Keller, W. Paciorek, P. Roversi, A. Sharff, O. S. Smart, C. Vonrhein, T. O. Womack, BUSTER (version 2.11.2), Global Phasing Ltd. (Cambridge, UK), **2016**.
[26] P. Emsley, B. Lohkamp, W. G. Scott, K. Cowtan, *Acta Crystallogr. Sect. D* **2010**, *66*, 486 – 501.
[27] S. S. Carroll, S. W. Ludmerer, L. Handt, K. Koeplinger, N. R. Zhang, D. Graham, M. E. Davies, M. MacCoss, D. J. Hazuda, D. B. Olsen, *Antimicrob. Agents Chemother.* **2009**, *53*, 926 – 934.
[28] J. M. Vrolijk, A. Kaul, B. E. Hansen, V. Lohmann, B. L. Haagmans, S. W. Schalm, R. Bartenschlager, *J. Virol. Methods* **2003**, *110*, 201 – 209.
[29] N. J. Liverton, S. S. Carroll, J. DiMuzio, C. Fandozzi, D. J. Hraham, D. Hazuda, M. K. Holloway, S. W. Ludmerer, J. A. McCauley, C. J. McIntyre, D. B. Olsen, M. T. Rudd, M. Stahlhut, J. P. Vacca, *Antimicrob. Agents Chemother.* **2010**, *54*, 305 – 311.
[30] K. J. Herlihy, J. P. Graham, R. Kumpf, A. K. Patick, R. Duggal, S. T. Shi, *Antimicrob. Agents Chemother.* **2008**, *52*, 3523 – 3531.

Manuscript received: April 10, 2017
Revised manuscript received: June 26, 2017
Accepted manuscript online: June 26, 2017
Version of record online: ■■ ■■, 0000

C. C. McComas, A. Palani, W. Chang, M. K. Holloway, C. A. Lesburg, P. Li, N. Liverton, P. T. Meinke, D. B. Olsen, X. Peng, R. M. Soll, A. Ummat, J. Wu, J. Wu, N. Zorn, S. W. Ludmerer*

■■ – ■■

Development of a New Structural Class of Broadly Acting HCV Non-Nucleoside Inhibitors Leading to the Discovery of MK-8876

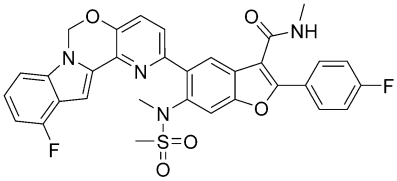

Both palms open: Studies directed at developing a broadly acting non-nucleoside inhibitor of HCV NS5B led to the discovery of a novel structural class of 5-aryl benzofurans that simultaneously interact with both the palm I and palm II binding regions. Herein we describe the efforts that led to the discovery of MK-8876, which advanced into Phase 1 monotherapy studies for evaluation and characterization as a component of an all-oral direct-acting drug regimen for the treatment of chronic HCV infection.